Soft-Decision Decoding in Noncoherent Massive MIMO Systems

George Yammine, Robert F.H. Fischer
Institut für Nachrichtentechnik, Universität Ulm, Ulm, Germany
Email: {george.yammine, robert.fischer}@uni-ulm.de

***Abstract*—Noncoherent multi-user detection schemes are attractive in massive MIMO uplink systems. In particular, sorted decision-feedback differential detection (DFDD) in combination with noncoherent decision-feedback equalization (nDFE) over the users has been shown to perform well, avoiding the need for channel estimation. So far, integrating channel coding in massive MIMO systems requires knowledge of the channel, where reliability information for the bits is calculated after combining a large number of symbol observations at the receiver. In this paper, we address one method to calculate reliability information by augmenting the sorted decision-feedback differential detection process. To this end, an equivalent trellis-encoder representation of bit-to-symbol mapping and differential encoding is established. Based on this, log-likelihood ratios for the differential symbols can be calculated. The performance of soft-decision decoding in noncoherent massive MIMO systems is assessed by means of numerical simulations and compared to that of a coherent scheme using channel estimation.**

I. Introduction

So-called *Massive MIMO* systems, where the base station is equipped with a very large number of receive antennas, have gained more and more attention [12], [14]. The drawback of such multiple-input/multiple-output (MIMO) systems is that the estimation of a huge number of channel coefficients is required, which quickly becomes challenging. This fact becomes even more severe if coded systems are considered, e.g., in recent publications [11], [5] schemes are given, which typically assume perfect knowledge of the channel coefficients, or employ complex iterative detection schemes.

In order to eliminate the need for channel estimation in a (multi-user) massive MIMO uplink system, one can resort to *noncoherent detection*. Noncoherent detection schemes based on exploiting the similarities between ultra-wideband (UWB) systems [15] and massive MIMO have been presented in [16], [7], where the performance for uncoded transmission was assessed. As in the coherent case, the obvious way to improve the performance of the system is to employ channel coding.

In this paper, we present a low-complexity method to calculate reliability information based on *decision-feedback differential detection (DFDD)*. To this end, an equivalent trellis encoder of the symbol-wise differential encoding scheme is established, based on which the reliability information after differential decoding, required by the channel decoder, can be calculated. This method is also extendable to the multi-user scenario, where the so-called *non-coherent decision-feedback equalization (nDFE)* [7] is employed to cope with the multi-user interference. The performance of this noncoherent detection scheme is assessed via numerical simulations.

This paper is organized as follows. In Sec. II, a brief review of the system model and noncoherent multi-user detection in massive MIMO is presented. Sec. III introduces the equivalent trellis encoder and the reliability information calculation method, and initial numerical simulation results are provided in Sec. IV. Finally, Sec. V provides a summary of the work and conclusions.

II. System Model and Noncoherent Detection

We consider a *multi-user uplink scenario* where N_u users (with a single antenna) simultaneously transmit to a central base station equipped with $N_\mathsf{rx} \gg 1$ antennas, illustrated in Fig. 1. In each time step k, user u transmits an M-ary differentially encoded PSK symbol $b_{k,u}$, which is generated from the PSK data symbols $a_{k,u}$ as

$$b_{k,u} = a_{k,u} b_{k-1,u} \ , \quad b_{0,u} = 1 \ . \tag{1}$$

Since the data symbols $a_{k,u}$ are drawn from the PSK signal set $\mathcal{M} \overset{\text{def}}{=} \{\mathrm{e}^{\mathrm{j}2\pi \cdot i/M} \mid i = 0, 1, \ldots, M-1\}$, the differentially encoded symbols $b_{k,u}$ are drawn from this set, too. In the receiver, noncoherent detection methods are applied, cf. Sec. II-B.

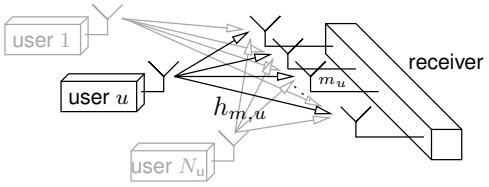

Fig. 1. Multi-user massive MIMO uplink system.

A. Geometric System Model

As in [16], a uniform linear array (antenna spacing d_a) is assumed at the receiver. The N_u users are located in front of the array; user u at a distance d_u and position m_u. Each antenna in the array exhibits a radiation pattern [18]

$$C(\psi) = \sqrt{G_\mathrm{i}} \cos(\psi \cdot N_\mathsf{notch}/2) \ , \tag{2}$$

where $N_\mathsf{notch} \in \mathbb{N}$ is the number of notches (nulls) in the pattern. The boresight (main lobe) of each individual antenna, $\psi = 0°$, is always perpendicular to the array and all boresights of each individual antenna are parallel to each other. The

boresight gain G_i is chosen such that the average received power seen by the antennas in the array is that of an omni-directional antenna, i.e., $G_\mathrm{i} = 2$. For an omni-direction antenna, we set $G(\psi) = 1$ and $N_\mathsf{notch} = 0$.

The discrete-time model (symbol interval T; equivalent complex baseband) of the individual channels between user u and antenna element m include pulse shaping at the transmitter, the continuous-time flat-fading channel (with attenuation, path loss, and fast fading), matched filtering, and symbol-spaced sampling at the receiver. Each channel coefficient $h_{m,u}$ is then given as

$$h_{m,u} = c_\mathrm{h} \cdot r_{m,u}^{-\gamma/2} \cdot C(\psi_{m,u}) \cdot h_{u,b,\mathrm{i.i.d.}} \,. \tag{3}$$

Here, $r_{m,u}^{-\gamma/2}$ is the path loss component (distance $r_{m,u}$, $\psi_{m,u}$ is the relative angle (cf. Fig. 2) between antenna m and user u, and *path loss exponent* γ). The i.i.d. zero-mean unit-variance complex Gaussian random variable $h_{u,b,\mathrm{i.i.d.}}$ accounts for fast fading effects due to scatterers in the vicinity of the user; c_h is a normalization constant. The channel model can be

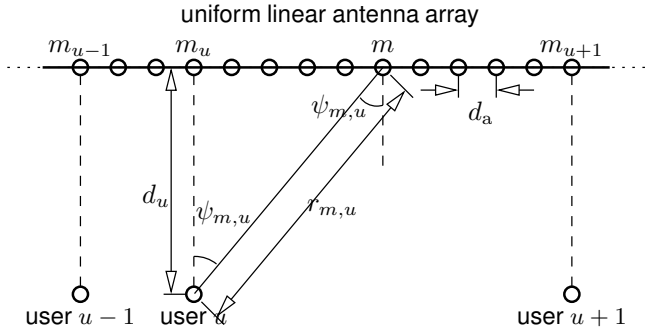

Fig. 2. Geometric system model for multi-user massive MIMO transmission.

specified via the average received power $P_{m,u}$ at each antenna m induced by user u, i.e., the *power-space profile (PSP)* [16]. Since $h_{m,u}$ is zero-mean, this calculates to (cf. [16], [18])

$$\begin{aligned} P_{m,u} &\overset{\text{def}}{=} \mathrm{E}\{|h_{m,u}|^2\} \qquad (4)\\ &= \mathrm{E}\{|c_\mathrm{h} \cdot r_{m,u}^{-\gamma/2} \cdot C(\psi_{m,u}) \cdot h_{u,b,\mathrm{i.i.d.}}|^2\} \\ &= c_\mathrm{p} \cdot \mathrm{e}^{-\gamma/2 \cdot \log(1+|m-m_u|^2/d_{\mathrm{r},u}^2)} \cdot |C(\psi_{m,u})|^2 \\ &\approx c_\mathrm{p} \cdot \mathrm{e}^{-|m-m_u|^2/(2\zeta^2)} \cdot |C(\psi_{m,u})|^2 \,, \qquad (5) \end{aligned}$$

where $d_{\mathrm{r},u} \overset{\text{def}}{=} d_u/d_\mathrm{a}$ is the relative distance (normalized to the antenna spacing) of the user u to the array; m_u and $d_{\mathrm{r},u}$ characterize the user; $c_\mathrm{p} = |c_\mathrm{h}|^2$ is a normalization constant. The quotient $\zeta^2 \overset{\text{def}}{=} d_{\mathrm{r},u}^2/\gamma$ is then used to describe the relative distance of the user u in relation to the path loss. The angle $\psi_{m,u}$ under which user u is seen by antenna m, calculates to

$$\psi_{m,u} = \tan^{-1}(|m - m_u|, d_{\mathrm{r},u}) \,, \tag{6}$$

using the 2-argument arc-tangent function, $\tan^{-1}(y, x)$, as can be seen from Fig. 2.

B. Noncoherent Detection

A block-fading channel model, where the fading coefficients $h_{m,u}$ are randomly chosen according to (3) and constant over a burst of size N_bl is assumed. *Multiple-symbol differential detection (MSDD)* [6] or its reduced-complexity version *decision-feedback differential detection (DFDD)* [1], [17] are applicable. We collect N_bl time steps (over the N_rx receive antennas) and form the receive block $\boldsymbol{R}$. It is given by [16]

$$\boldsymbol{R} = \sum\nolimits_{u=1}^{N_\mathsf{u}} \boldsymbol{h}_u \boldsymbol{b}_u + \boldsymbol{N} \,, \tag{7}$$

where $\boldsymbol{h}_u \overset{\text{def}}{=} [h_{1,u}, \ldots, h_{N_\mathsf{rx},u}]^\mathsf{T}$ is the (column) vector of channel coefficients for user u and $\boldsymbol{b}_u \overset{\text{def}}{=} [b_{0,u}, \ldots, b_{N_\mathsf{bl}-1,u}]$ is the (row) vector of transmit symbols of user u. The matrix $\boldsymbol{N}$ collects the circular-symmetric complex Gaussian noise $n_{m,k}$ with zero mean and variance σ_n^2.

Differential detection of the symbols of user u can then be based on the $N_\mathsf{bl} \times N_\mathsf{bl}$ *correlation matrix*

$$\boldsymbol{Z}_u \overset{\text{def}}{=} \boldsymbol{R}^\mathsf{H} \boldsymbol{W}_u \boldsymbol{R} \,, \tag{8}$$

using the user-specific diagonal weighting matrix

$$\boldsymbol{W}_u \overset{\text{def}}{=} \mathbf{diag}(w_{1,u}, \ldots, w_{N_\mathsf{rx},u}) \,. \tag{9}$$

The operation of DFDD in the massive MIMO scenario was introduced in [16]. After the calculation of the correlation matrix $\boldsymbol{Z}$ (user index u is omitted for readability), decisions are generated successively, taking all previously detected symbols into account. Specifically, the index $\hat{k}_n$ of the symbol to be detected next is given by

$$\hat{k}_n = \underset{\substack{\bar{k}\in\{1,\ldots,N_\mathsf{bl}-1\}\\ /\{\hat{k}_1,\ldots,\hat{k}_{n-1}\}}}{\operatorname{argmin}} \left| \Delta\mathcal{Q}_\mathsf{PSK} \left\{ \sum_{l=0}^{n-1} \hat{b}_{\hat{k}_l}^\mathsf{DFDD} z_{\bar{k},\hat{k}_l} \right\} \right| \,, \tag{10}$$

and the decision of this symbol is obtained as

$$\hat{b}_{\hat{k}_n}^\mathsf{DFDD} = \mathrm{e}^{\mathrm{j}\mathcal{Q}_\mathsf{PSK}\left\{\sum_{l=0}^{n-1} \hat{b}_{\hat{k}_l}^\mathsf{DFDD} z_{\hat{k}_n,\hat{k}_l}\right\}} \,, \quad n = 1, \ldots, N_\mathsf{bl} - 1 \,, \tag{11}$$

with $\hat{k}_0 = 0$ and $\hat{b}_0^\mathsf{DFDD} = 1$. Thereby,[1]

$$\mathcal{Q}_\mathsf{PSK}\{x\} \overset{\text{def}}{=} \frac{2\pi}{M} \cdot \left\lfloor \frac{M}{2\pi} \cdot \arg(x) \right\rceil \tag{12}$$

denotes the M-ary phase quantization and

$$\Delta\mathcal{Q}_\mathsf{PSK}\{x\} \overset{\text{def}}{=} \mathrm{mod}_{\mathrm{s},2\pi}\big(\arg(x) - \mathcal{Q}_\mathsf{PSK}(x)\big) \tag{13}$$

calculates the quantization error. Since the first detected symbols are not reliable due to not having enough feedback information, a performance increase can be obtained by revisiting those first detected symbols and using the $N_\mathsf{bl} - 1$ feedback of the latter symbols in redetecting them.

To cope with multi-user interference, *noncoherent decision-feedback equalization (nDFE)* over the users can be applied [7], by which significant performance improvements can be obtained. The main idea behind nDFE is the subtraction of

[1] $\lfloor\cdot\rceil$: rounding to the next integer. $\mathrm{mod}_{\mathrm{s},2\pi}$: symmetrical modulo operation, i.e., reduction into the interval $(-\pi, +\pi]$.

the the interference caused by the already detected users. To this end, the data symbols (of the previously detected users) and the channel coefficients have to be known [9]. In the case of noncoherent detection, the latter is not known, but rather statistics about the channel coefficients are known via the PSP. The detection order can be sorted optimally based on the *signal-to-noise-plus-interference ratio (SINR)* of the individual users. A sufficiently accurate approximation was derived in [7]. For user u it reads

$$\mathrm{SINR}_u = \frac{\eta_{u,u}^2 + \sigma_{u,u,u}^2}{\sum\limits_{\nu \notin \mathcal{D}, \nu \neq u} \eta_{u,\nu}^2 + \sum\limits_{(\nu,\mu) \neq (u,u)} \sigma_{u,\nu,\mu}^2 + \sigma_{\mathrm{n},u}^2} \ , \quad (14)$$

where $\mathcal{D}$ is the index set of the already detected users and

$$\eta_{u,\nu} \stackrel{\text{def}}{=} \sum\nolimits_{m=1}^{N_{\mathsf{rx}}} w_{m,u} P_{m,\nu} \ , \quad (15)$$

$$\sigma_{u,\nu,\mu}^2 \stackrel{\text{def}}{=} \sum\nolimits_{m=1}^{N_{\mathsf{rx}}} w_{m,u}^2 P_{m,\nu} P_{m,\mu} \ , \quad (16)$$

$$\sigma_{\mathrm{n},u}^2 \stackrel{\text{def}}{=} \sum\nolimits_{m=1}^{N_{\mathsf{rx}}} w_{m,u}^2 \big(\sigma_{\mathsf{n}}^4 + 2\sigma_{\mathsf{n}}^2 \sum\nolimits_{\nu=1}^{N_{\mathsf{u}}} P_{m,\nu}\big) \ . \quad (17)$$

Looking at the SINR reveals that it only depends on the PSP $P_{m,u}$ and the weighting factors $w_{m,u}$ of the user being detected, the PSPs $P_{m,\nu}$, $P_{m,\mu}$ of the interfering users and the noise variance σ_{n}^2 (we assume it to be known).

Given the PSP, the weighting factors $w_{m,u}$ can be adjusted in order to maximize the SINR of each user individually. Given the optimum decision order and the weighting factors of the individual users, we can then apply nDFE

$$\boldsymbol{z}_u' = \boldsymbol{z}_u - \sum_{\nu \in \mathcal{D}} \eta_{u,\nu} \left(\hat{\boldsymbol{b}}_\nu^{\mathsf{DFDD}}\right)^{\mathsf{H}} \hat{\boldsymbol{b}}_\nu^{\mathsf{DFDD}} \ , \quad (18)$$

by which the mean interference from the already detected user ν is subtracted. When applying DFDD, the correlation matrix $\boldsymbol{Z}_u'$ is then used instead of the conventional correlation matrix $\boldsymbol{Z}_u$. DFDD/nDFE establishes a low-complexity but well-performing strategy for noncoherent multi-user detection.

III. Equivalent Differential Encoding and Reliability Information Calculation

The process of differential encoding is depicted in Fig. 3 (top). For brevity, we restrict the exposition to $M = 4$-ary PSK and drop the user index u for readability. In view of binary channel coding, *Gray labeling* of the PSK symbols is assumed.

The vector of input bits $\boldsymbol{c}_k \stackrel{\text{def}}{=} [c_{1,k}\ c_{0,k}]$ is mapped to 4-ary PSK symbols $a_{k,u}$ (cf. Fig. 4). These are then differentially encoded, i.e.,

$$b_k = a_k b_{k-1} \ , \quad b_0 = 1 \ , \quad (19)$$

to obtain the transmit symbols.

Noteworthy, if *natural labeling* ($\mathcal{M}_{\mathsf{nat}}$) is used, the differential encoding process can equivalenty be described via modulo-M addition of the bit label (interpreted as an integer) followed by mapping. Fortunately, via preprocessing of the bit labels ($[c_{1,k}\ c_{0,k}] \ \rightarrow \ [c_{1,k}\ c_{1,k} \oplus c_{0,k}]$, where $\oplus$ denotes addition modulo 2) natural labeling can be transformed into Gray labeling and vice versa. This gives rise to the block diagram in the middle row of Fig. 3.

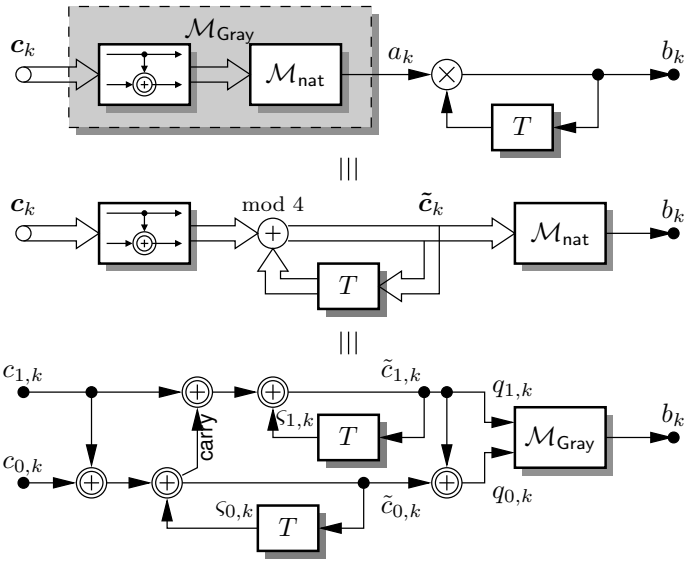

Fig. 3. Different descriptions of differential encoding and mapping. Top: bit-to-symbol mapping followed by differential encoding. Middle: differential encoding using modulo-4 addition followed by mapping. Bottom: differential encoding described by an 4-state rate-1 trellis encoder followed by mapping using Gray labeling. Additions with double line symbolize modulo 2 addtions. The user index u is dropped for readability.

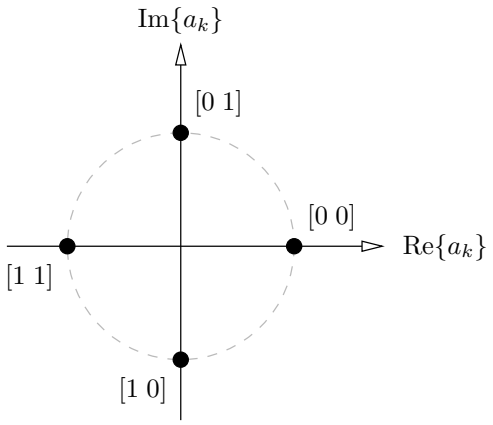

Fig. 4. Graphical representation of bit-to-symbol mapping of 4-PSK using Gray labeling. The labeling order used is $[c_{1,k}\ c_{0,k}]$.

Finally, combining the transformations of the mappings and the accumulation structure, in the bottom row of Fig. 3 the differential encoding/mapping process is shown as employing a rate-1 trellis encoder with 4 states. The bit vector $\boldsymbol{c}_k$ is encoded into the bit vector $\boldsymbol{q}_k$, which is then mapped to the 4-ary PSK symbols b_k, cf. [13]. This procedure can be applied to any cardinality M of the PSK symbols.

Having the equivalent encoder in Fig. 3, a trellis diagram describing the action of the encoder can be stated. Given the current state $[\varsigma_{1,k}\ \varsigma_{0,k}]$ (the vector $[\tilde{c}_{1,k}\ \tilde{c}_{0,k}]$ of the previous step) an input vector $[c_{1,k}\ c_{0,k}]$ causes a current output vector $[q_{1,k}\ q_{0,k}]$ and a new state. The diagram for the $M = 4$-ary differential PSK transmission at hand can be seen in Fig. 5.

At the receiver side, using the equivalent trellis code representation of differential encoding, we can then differentially decode soft-bit information, e.g., log-likelihood ratios (LLRs) by employing soft-input/soft-output decoding algorithms, such as the BCJR algorithm [2].

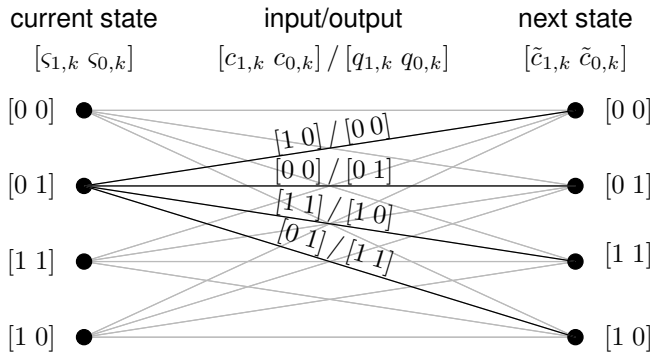

Fig. 5. Trellis diagram describing differential encoding and Gray labeled 4-PSK transmission. Only the paths from state [0 1] are shown for readability.

A. Reliability Information Calculation

Using the equivalent bit-wise differential encoding model, calculating the LLRs of the differentially encoded symbols can be then done in two steps. To that end, we resort to the (sorted) DFDD process itself. In doing so, we calculate the LLRs using the feedback, normalized to the unit circle (cf. Fig. 6) since relevant information is only in the phase of the received symbols (see (11))

$$\breve{b}_{\hat{k}_n}^{\mathsf{DFDD}} = \frac{\sum_{l=0}^{n-1} \hat{b}_{\hat{k}_l}^{\mathsf{DFDD}} z_{\hat{k}_n,\bar{k}_l}}{\left|\sum_{l=0}^{n-1} \hat{b}_{\hat{k}_l}^{\mathsf{DFDD}} z_{\hat{k}_n,\bar{k}_l}\right|}\ , \quad n = 1,\ldots,N_{\mathsf{bl}}-1\ . \tag{20}$$

The calculation order follows the same optimum decision order as for the DFDD process.

Given the entire block of symbols $\breve{b}_{\hat{k}_n}^{\mathsf{DFDD}}$, the LLR calculation is then

$$L_{q_{i,k}} = \log\left(\frac{\sum_{s_j\in\mathcal{S}_i^0} \mathrm{e}^{-\left|\breve{b}_k^{\mathsf{DFDD}}-s_j\right|^2/\sigma_{\mathsf{n}}^2}}{\sum_{s_j\in\mathcal{S}_i^1} \mathrm{e}^{-\left|\breve{b}_k^{\mathsf{DFDD}}-s_j\right|^2/\sigma_{\mathsf{n}}^2}}\right)\ , \quad k = 1,\ldots,N_{\mathsf{bl}}-1\ , \tag{21}$$

where $\mathcal{S}_i^0$, $\mathcal{S}_i^1$ are the sets of symbols where the bit $q_{i,k}$, $i = 0,1$ is zero or one respectively, and $\hat{b}_0^{\mathsf{DFDD}} = 1$. The obtained LLRs on the bit representing the differentially encoded symbols b_k can be then differentially decoded via the BJCR algorithm, operating on the above described trellis of the differential encoder, to obtain the LLRs for the bits $c_{i,k}$ ($L_{q_{i,k}} \xrightarrow{\mathsf{BCJR}} L_{c_{i,k}}$).

B. Reliability Information Calculation Based on Angles

An alternative, on first glance more natural, method to calculate the reliability information of the differentially encoded symbols, is to use the argument of the observed (normalized) feedback symbols of the DFDD process. Assuming that the noise in the angle is real Gaussian distributed (cf. Fig. 6) with zero mean and variance $\sigma_{\mathsf{n}}^2/2$, the LLR reads

$$L_{q_{i,k}} = \log\left(\frac{\sum_{\theta_j\in\Theta_i^0} \mathrm{e}^{-(\mathrm{mod}_{\mathrm{s},2\pi}(\phi_k-\theta_j))^2/\sigma_{\mathsf{n}}^2}}{\sum_{\theta_j\in\Theta_i^1} \mathrm{e}^{-(\mathrm{mod}_{\mathrm{s},2\pi}(\phi_k-\theta_j))^2/\sigma_{\mathsf{n}}^2}}\right)\ , \quad k = 1,\ldots,N_{\mathsf{bl}}-1\ , \tag{22}$$

where $\phi_k \overset{\mathrm{def}}{=} \arg\left(\breve{b}_k^{\mathsf{DFDD}}\right)$ is the argument of the observation, Θ_i^b is the set of angles of the symbols of the M-PSK alphabet with bit $b = 0,1$ at position i, respectively.

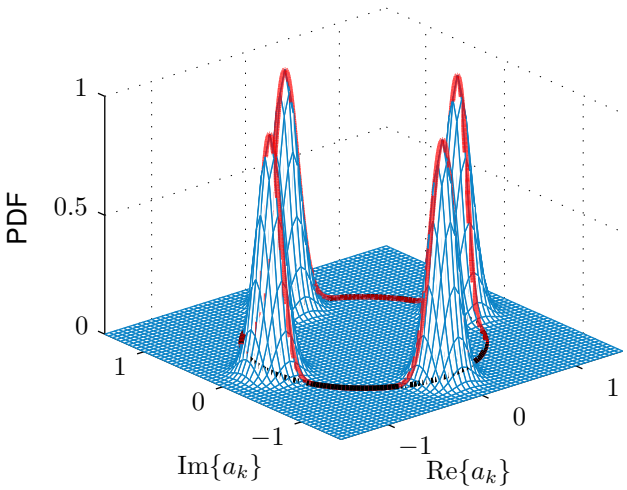

Fig. 6. Illustration describing the effect of normalizing the received symbols plus noise to the unit circle. Blue: 4-PSK symbols with complex valued Gaussian noise. Red: normalized symbols plus noise. Black: unit circle.

IV. Numerical Simulations

For assessment, numerical simulations were conduced using two different scenarios, an $N_{\mathsf{u}} = 1$ single-user scenario, and an $N_{\mathsf{u}} = 3$ multi-user scenario, both with an $N_{\mathsf{rx}} = 100$ uniform linear antenna array with omni-directional antennas ($N_{\mathsf{notch}} = 0$). A relative distance $d_{\mathrm{r},u} = 38$ and propagation constant $\gamma = 3.6$ were chosen, resulting in $\zeta = 20$. The PSP is calculated according to (5) and then is normalized for an average total receiver power of one.

A. Single-User Scenario

For transmission, the information bits are first encoded using a binary LDPC code [4] and then randomly interleaved. In the noncoherent case, a rate-1/2 length $n_{\mathsf{c}} = 800$, dimension $k_{\mathsf{c}} = 400$ LDPC code is employed. The coded bits are then mapped to a $M = 4$-PSK alphabet using Gray labeling. The resultant block of 400 symbols is then segmented into blocks of length of $N_{\mathsf{data}} = 200$; in the present case two transmission bursts result for each coded block. A reference symbol (w.l.o.g.) $b_0 = 1$ is appended to each of the segmented blocks, which are then differentially encoded, which results in a transmission burst of length $N_{\mathsf{bl}} = 201$. Equivalently the

coded bits can be differentially encoded using the $M = 4$-state rate-1 trellis encoder and then mapped to the 4-ary PSK alphabet and segmented into two bursts for transmission.

In the coherent case, the coded bits are mapped onto the 4-PSK symbol alphabet using Gray labeling, and then segmented into blocks taking into consideration the addition of a training sequence at the start of each segment. In the numerical simulation, a training sequence length of 25% of the block length was chosen, which was shown to be optimum in [8]. For a fair comparison, both systems should have the same end-to-end information rate, i.e., the same amount of information is represented in the same number of transmission bursts. Hence, a code with shorter length and higher rate must be employed. Here, the used LDPC code is a rate-2/3 length $n_{\mathsf{c}} = 600$, dimension $k_{\mathsf{c}} = 400$ code. A graphical representation of the encoding, mapping, segmentation, and the appending of the reference symbol (noncoherent case) and training sequence (coherent case) can be seen in Fig. 7.

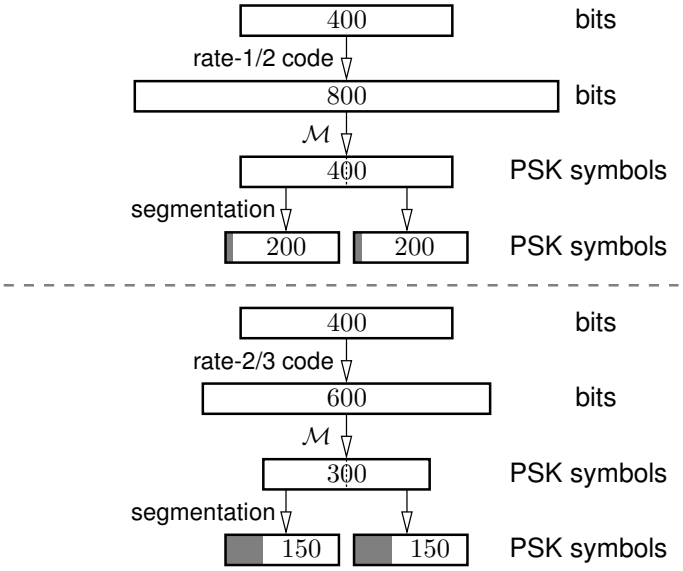

Fig. 7. Graphical representation of the encoding and mapping process. Top: noncoherent case. 400 information bits are encoded using a rate-1/2 code. The coded bits are then mapped ($\mathcal{M}$) onto 4-PSK symbols. The obtained PSK symbols are segmented to two bursts and one reference symbol is appended for differential encoding. Bottom: coherent case. 400 information bits are encoded using a rate-2/3 code. The coded bits are then mapped ($\mathcal{M}$) onto 4-PSK symbols. The obtained PSK symbols are segmented to two bursts and a training sequence of length of 25% of the block length is appended. Shaded areas represent the appended reference symbol and training sequence respectively.

At the receiver side, in the noncoherent case, the correlation matrix $\boldsymbol{Z}$ is first calculated, and then used to calculate the LLRs of the coded bits according to (21). It is worth noting that using (21) or calculating the reliability information based on the argument (22), results in almost the same performance (cf. Fig. 8), however the latter requires a higher computational complexity. The LLRs are then differentially decoded using the BCJR algorithm, which are then decoded to retrieve the information bits.

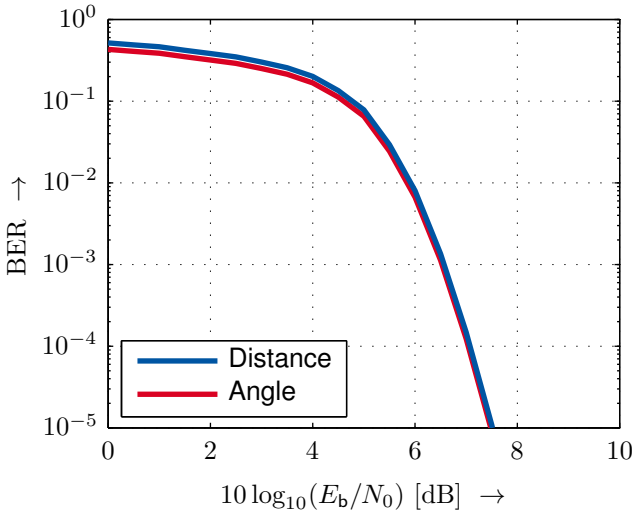

Fig. 8. Bit-error rate vs. E_{b}/N_0 (in dB). Single-user scenario. Uniform linear array with $N_{\mathsf{rx}} = 100$ antenna elements; omni-directional. Power-space profile according to (5) with $\zeta = 20$. Burst length $N_{\mathsf{bl}} = 201$. Blue: noncoherent (DFDD + LLR calc. based on distance as given in (21) with rate-1/2, length $n_{\mathsf{c}} = 800$, dimension $k_{\mathsf{c}} = 400$ LDPC code. Red: noncoherent (DFDD + LLR calc. based on angles as given in (22) with rate-1/2, length $n_{\mathsf{c}} = 800$, dimension $k_{\mathsf{c}} = 400$ LDPC code.

In the coherent case, the training sequence, part of each block, is first extracted, and then used to estimate the channel using a linear least-squares estimator. Matched filtering, i.e., maximum-ratio combining is then performed using the estimated channel coefficients, and then reliability information is calculated, based on the AWGN assumption, which in this case is optimal.

The numerical results (cf. Fig. 9) show that using the low-complexity noncoherent scheme, where the LLR calculation is performed based on the DFDD process (in red) provides a very good performance in comparison to the coherent case (in blue). The bit-error rate of uncoded transmission for the noncoherent case (detection using DFDD) and coherent case are provided (dashed) for reference. One can also note that for a given bit-error-rate, the performance gap between the coded systems is smaller than the performance gap of the uncoded systems. This performance gain comes from the stronger rate-1/2 LDPC code that was employed, which cannot be used in the coherent case, since an overhead for the training sequence limits the code length.

B. Multi-User Scenario

In the multi-user scenario case, $N_{\mathsf{u}} = 3$ users are distributed in front of the same $N_{\mathsf{rx}} = 100$ linear array using omni-directional antennas (relative distance $d_{\mathrm{r},u} = 38$ and propagation exponent $\gamma = 3.6$), as in the single-user scenario case. User 1 (■), user 2 (■) and user 3 (■) are placed in front of antennas $m_1 = 20$, $m_2 = 50$ and $m_3 = 85$, respectively. The PSPs are calculated according to (5) and the PSP of each user is normalized for an average total receiver power of one.

For transmission, each user encodes its own information

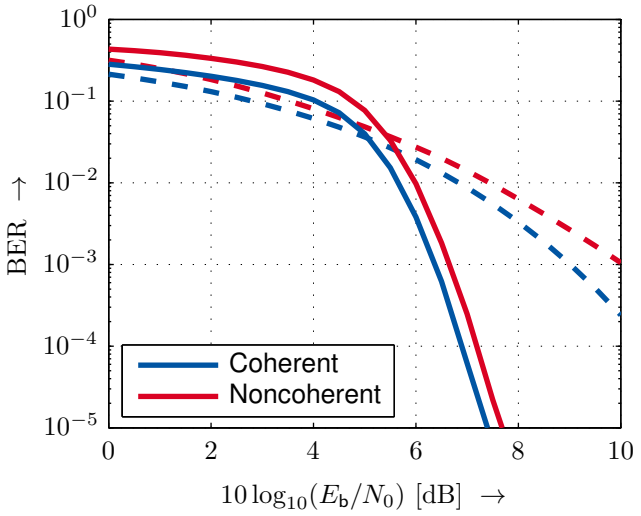

Fig. 9. Bit-error rate vs. E_b/N_0 (in dB). Single-user scenario. Uniform linear array with $N_{rx} = 100$ antenna elements; omni-directional. Power-space profile according to (5) with $\zeta = 20$. Burst length $N_{bl} = 201$. Blue: coherent (ch. est. + MRC + LLR calc. based on AWGN assumption) with rate-2/3, length $n_c = 600$, dimension $k_c = 400$ LDPC code. Red: noncoherent (DFDD + LLR calc. as given in 21) with rate-1/2, length $n_c = 800$, dimension $k_c = 400$ LDPC code. Dashed: uncoded transmission.

bits using the same binary LDPC code, and then the code bits are individually randomly interleaved. In the noncoherent case, the same rate-1/2 code of length $n_c = 800$ and dimension $k_c = 400$ is employed, and the process of mapping, segmentation, and block formation (by appending a reference symbol and differentially encoding each block) is performed. In the coherent case, each user is assigned a distinct training sequence from a set of orthogonal sequences. To this end, constant-amplitude zero-autocorrelation orthogonal sequences, here, Zadoff-Chu sequences [3], [10], were employed. Similar to the single-user case, a rate-2/3 length $n_c = 600$ dimension $k_c = 400$ binary LDPC code was employed.

The numerical results for the multi-user scenario case can be seen in Fig. 10. We can directly see that the performance of noncoherent detection in this case is worse than that of coherent detection. The interference of the users in close proximity to each other is reduced by nDFE, however a large portion of it still hinders the detection process. It is noteworthy that the user farthest (in terms of location in front of the array) from the others, here user 3 (■), has the best performance of the three. In terms of PSPs, user 3 has the lowest amount of overlap among all three.

One method to improve the performance of noncoherent detection in massive MIMO systems is to employ at the base station, antennas with some directional properties [18]. Using antennas with $N_{notch} = 4$ instead of omni-directional antennas, the overlap in the PSPs of the users is lowered, hence the interference caused by neighboring users is reduced, and the gap between coherent and noncoherent detection is decreased, as can be seen in Fig. 11, approaching the results of the single-user scenario. It is also worth noting that the channel code used is designed for the AWGN channel, which expects the LLR to be Gaussian distributed. However in the case of the multi-user scenario with noncoherent detection, the LLRs are not Gaussian distributed and thus the LDPC code in use is not optimal.

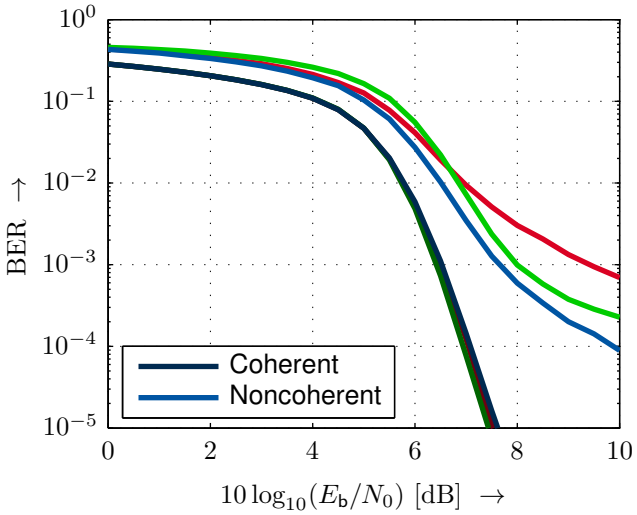

Fig. 10. Bit-error rate vs. E_b/N_0 (in dB). Multi-user scenario. $N_u = 3$; $m_1 = 20$ (■), $m_2 = 50$ (■), $m_3 = 85$ (■). Uniform linear array with $N_{rx} = 100$ antenna elements; omni-directional. Power-space profile according to (5) with $\zeta = 20$. Burst length $N_{bl} = 201$. Coherent (ch. est. + MRC + LLR calc. based on AWGN assumption) with rate-2/3, length $n_c = 600$, dimension $k_c = 400$ LDPC code. Noncoherent (DFDD + LLR calc. as given in 21) with rate-1/2, length $n_c = 800$, dimension $k_c = 400$ LDPC code.

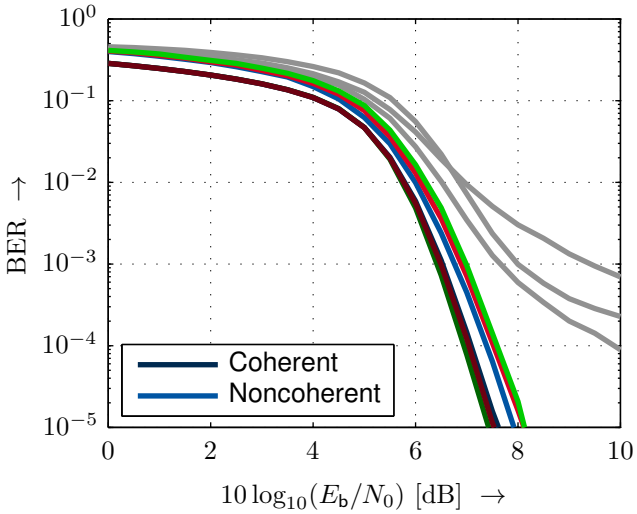

Fig. 11. Bit-error rate vs. E_b/N_0 (in dB). Multi-user scenario. $N_u = 3$; $m_1 = 20$ (■), $m_2 = 50$ (■), $m_3 = 85$ (■). Uniform linear array with $N_{rx} = 100$ antenna elements; $N_{notch} = 4$. Power-space profile according to (5) with $\zeta = 20$. Burst length $N_{bl} = 201$. Coherent (ch. est. + MRC + LLR calc. based on AWGN assumption) with rate-2/3, length $n_c = 600$, dimension $k_c = 400$ LDPC code. Noncoherent (DFDD + LLR calc. as given in 21) with rate-1/2, length $n_c = 800$, dimension $k_c = 400$ LDPC code. Gray: reference results of base station using omni-directional antennas.

V. Conclusions

In this work, we have shown a low-complexity method to calculate reliability information for soft-decision decoding in noncoherent massive MIMO systems. We have shown using numerical simulations the performance of this suboptimal method is comparable to coherent detection using maximum-ratio combining. It is important to note that the performance of noncoherent soft-decision detection can be further improved by employing codes that are optimized for use in this scenario, or by warping the LLRs. Alternative solutions to improve the performance would be employing antennas with advantageous properties, or by using iterative techniques, such as iterative demapping and decoding.

References

[1] F. Adachi, M. Sawahashi. Decision-Feedback Multiple-Symbol Differential Detection for Mary DPSK. *Electronics Letters*, pp. 1385–1387, July 1993.

[2] L.R. Bahl, J. Cocke, F. Jelinek, J. Raviv. Optimal Decoding of Linear Codes for Minimizing Symbol Error Rate *IEEE Trans. Inf. Theory*, vol. 20, pp. 284–287, March 1974.

[3] D. Chu. Polyphase Codes with Good Periodic Correlation Properties (Corresp.). *IEEE Trans. Inf. Theory*, pp. 531–532, Jul. 1972.

[4] L. Costantini, B. Matuz, G. Liva, E. Paolini, M. Chiani. Non-Binary Protograph Low-Density Parity-Check Codes for Space Communications. *International Journal of Satellite Communications and Networking*, pp. 43–51, 2012.

[5] X. Dai, R. Zou, S. Sun, Y. Wang. Reducing the Complexity of Quasi-ML Detectors for MIMO Systems Through Simplified Branch Metric and Accumulated Branch Metric Based Detection *IEEE Communication Letters*, pp. 916–919, May 2013.

[6] D. Divsalar, M.K. Simon. Multiple-Symbol Differential Detection of MPSK. *IEEE Trans. Communications*, pp. 300–308, Mar. 1990.

[7] R.F.H. Fischer, M. Bense. Noncoherent Decision-Feedback Equalization in Massive MIMO Systems. In *Proceedings of International Zurich Seminar (IZS)*, pp. 112–115, Zurich, Switzerland, Feb. 2014.

[8] R.F.H. Fischer, M. Bense, C. Stierstorfer. Noncoherent Joint Decision-Feedback Detection in Multi-User Massive MIMO Systems. In *Proceedings of International ITG/IEEE Workshop on Smart Antennas*, Erlangen, Germany, Mar. 2014.

[9] G.J. Foschini, D. Chizhik, M.J. Gans, C. Papadias, R.A. Valenzuela. Analysis and Performance of Some Basic Space-Time Architectures. *IEEE J. Sel. Areas in Communications*, pp. 303–320, Apr. 2003.

[10] R. Frank. Polyphase Codes with Good Nonperiodic Correlation Properties. *IEEE Trans. Inf. Theory*, pp. 43–45, Jan. 1963.

[11] P. Li, R.C. de Lamare, R. Fa. Multiple Feedback Successive Interference Cancellation Detection for Multiuser MIMO Systems *IEEE Trans. Wireless Communications*, pp. 2434–2439, Aug. 2011.

[12] T.L. Marzetta. Noncooperative Cellular Wireless with Unlimited Numbers of Base Station Antennas. *IEEE Trans. Wireless Communications*, pp. 3590–3600, Nov. 2010.

[13] P.J. McLane, P.H. Wittke, P.K.-M. Ho, C. Loo. PSK and DPSK Trellis Codes for Fast Fading, Shadowed Mobile Satellite Communication Channels *IEEE Tran. Communications*, pp. 1242–1246, Nov. 1988.

[14] F. Rusek, D. Persson, B.K. Lau, E.G. Larsson, T.L. Marzetta, O. Edfors, F. Tufvesson. Scaling Up MIMO: Opportunities and Challenges with Very Large Arrays. *IEEE Signal Processing Magazine*, pp. 40–60, Jan. 2013.

[15] A. Schenk. *Coding, Modulation, and Detection in Impulse-Radio Ultra-Wideband Communications*, PhD Thesis. University Erlangen-Nürnberg, 2012.

[16] A. Schenk, R.F.H. Fischer. Noncoherent Detection in Massive MIMO Systems. In *Proceedings of International ITG/IEEE Workshop on Smart Antennas*, Stuttgart, Germany, Mar. 2013.

[17] R. Schober, W.H. Gerstacker, J.B. Huber. Decision-Feedback Differential Detection of MDPSK for Flat Rayleigh Fading Channels. *IEEE Trans. Communications*, pp. 1025–1035, July 1999.

[18] G. Yammine, R.F.H. Fischer, C. Waldschmidt. On the Influence of the Antenna Pattern in Noncoherent Massive MIMO Systems In *Proceedings of The Twelfth International Symposium on Wireless Communication Systems*, Brussels, Belgium, Aug. 2015.